Theory and Analysis of the 'Super Whistler'

P. A. BERNHARDT

Radioscience Laboratory, Stanford University, Stanford, California 94305

Whistlers observed on the ground with frequency cutoffs greater than one-half the equatorial electron gyrofrequency along their field-aligned propagation paths have been termed super whistlers. The rarity of the super whistler is a consequence of the relatively small number of ducts which allow their propagation. The upper cutoff frequency of the super whistler is directly related to the physical structure of the duct. In addition to the path location and equatorial electron density that can be deduced from ordinary whistlers, super whistlers also provide information on density gradients along the magnetic field lines near the equator. Analysis of one set of super whistlers shows that immediately after a magnetic disturbance the equatorial plasma near $L = 4.5$ is in an intermediate state between the collisionless and diffusive equilibrium distributions. The plasma distribution approaches that of diffusive equilibrium after a period of low geomagnetic activity.

1. INTRODUCTION

The whistler is a natural VLF signal generated by a lightning stroke (or spheric) which propagates in the magnetosphere. A whistler may be guided by enhanced plasma columns to the conjugate hemisphere, and is then said to be 'ducted.' The signal contains information about the structure of the magnetosphere. The frequency versus time measurements of the whistler may be used to estimate some parameters of the plasma distribution along the field-aligned path. The accuracy of this estimation is limited by the signal-to-noise ratio of the whistler data [*Smith*, 1960].

One measurable feature of a whistler is its upper cutoff frequency. Above this frequency the amplitude of the whistler drops below a detectable level. The ratio of the cutoff frequency to the equatorial electron gyrofrequency along the propagation path is denoted by $\Lambda = f_c/f_{Heq}$ where f_c is the whistler cutoff frequency and f_{Heq} is the equatorial electron gyrofrequency of the path. If the whistler cutoff is well below the whistler nose frequency, it is of little use for magnetospheric plasma density estimations. Whistlers which cut off above the nose (called nose whistlers) can provide estimates of the L shell of the propagation path as well as the equtorial electron concentration along the path [*Park*, 1972]. Nose frequency analysis uses a predetermined plasma model to estimate the L shell, equatorial concentration, and flux tube content. This analysis does not provide any information about the field-line distribution of plasma. Much work has been done to develop curve-fitting techniques to estimate the nose frequency of non-nose whistlers [*Dowden and Allcock*, 1971; *Bernard*, 1973; *Ho and Bernard*, 1973; *Smith et al.*, 1975; *Tarcsai*, 1975; *Corcuff*, 1977; *Corcuff et al.*, 1977].

The classical theory of ducted whistler propagation [*Smith et al.*, 1960] predicts that the cutoff frequency of a whistler should equal one-half the equatorial gyrofrequency (i.e., $\Lambda \leq 0.5$) along the propagation path. A study of measured whistler components yielded a value of $\Lambda = 0.51 \pm 0.03$ [*Carpenter*, 1968]. The information content of such a whistler is only slightly greater than that of a whistler that is cut off at the nose frequency. Consequently, routine analysis of common whistlers can only provide the propagation path L shell and the equatorial plasma concentration.

In rare instances, whistlers with extraordinarily high cutoff frequencies have been recorded. These whistlers with $\Lambda > 0.6$ have been termed 'super whisters.' The existence of the super whistler is explained here in terms of a field-aligned enhancement (duct) which has the proper physical characteristics for guiding above the half electron gyrofrequency at the equator. Thus the super whistler is thought to be a ducted phenomenon, not a triggered emission.

This paper presents a discussion of VLF radio wave propagation which accounts for both the rarity and the high frequency characteristics of the super whistler. Following this discussion we describe a technique for obtaining additional information about the magnetospheric plasma distribution from the extraordinarily high-frequency components in the whistler.

2. WAVE GUIDING IN MAGNETOSPHERIC DUCTS

The requirements for ducting between geomagnetically conjugate ground stations is much less restrictive for frequencies below the equatorial half-gyrofrequency than for propagation above this frequency. To illustrate this, a new method of describing the propagation characteristics of a duct is formulated.

Previous studies of magnetospheric wave guiding have used theoretical arguments in conjunction with limited raytracing calculations [*Smith et al.*, 1960; *Helliwell*, 1965]. This study involves the propagation of a multitude of rays with a spectrum of wave-normal angles and injection altitudes at the equator. A modified version of the two-dimensional raytracing program described by *Walter* [1969] is used in this research.

One objective of this study is to demonstrate the existence of ducts which allow interhemispherical propagation for whistler-mode waves with frequencies greater than $0.6f_{Heq}$. For simplicity, this is a two-dimensional study, and the investigation is limited to rays propagating in the magnetic meridional plane centered on the duct.

This research is only concerned with conditions necessary for VLF propagation across the equator. Propagation effects near the duct endpoints are beyond the scope of the present work. Endpoint effects would complicate the analysis because (1) duct endpoint heights fluctuate with time [*Bernhardt and Park*, 1977], (2) signals originating from the gound can enter at the sides or the ends of the ducts [*Strangeways*, 1977], and (3) refraction by F region and E region plasma gradients can affect the transmission of VLF waves through the bottomside ionosphere. Our studies of VLF leakage from ducts show that it is necessary for rays to be ducted below 1600-km altitude to be received on the ground. Thus if a downward propagating ray leaves a duct with a geocentric radius greater than 1.25

Paper number 9A0496.
0148-0227/79/009A-0496$01.00

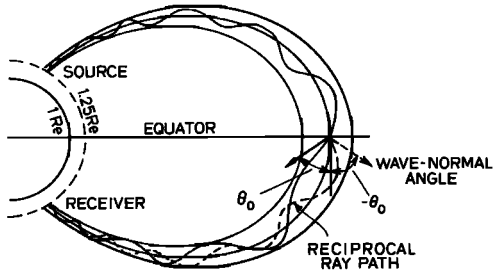

Fig. 1. Schematic of VLF ray propagation between hemispheres. The wave normal of the ray makes an angle of θ_0 degrees with the magnetic field at the equator.

earth radii (R_e), it is assumed that the ray cannot reach the ground. If, however, the ray is guided downward below 1.25 R_e, it may penetrate the bottomside ionosphere to the ground, depending on the F region plasma gradients, the duct endpoint heights, etc.

In this study, rays are injected at the equator rather than from the ground for two reasons. First, as mentioned above, the effects near duct endopints are not considered here. Second, knowledge of the trajectories of rays originating at the equator provides the information required to determine if interhemispheric propagation (at least to 1.25 R_e) can be achieved. This statement is justified in the following paragraph.

Consider the guiding of a VLF ray as illustrated by the solid, snake-like curve in Figure 1. The wave normal angle (WNA) at the equator is θ_0. Consequently, a ray injected at the equator with wavenormal θ_0 at the position in the duct shown in Figure 1 will be guided below 1.25 R_e. If the duct is symmetric about the equator, then, by reciprocity, a ray injected with wavenormal angle $-\theta_0$ (dashed curve in Figure 1) will also be guided below 1.25 R_e. Therefore a necessary condition for interhemispheric propagation is that if a ray injected at the equator with θ_0 degrees wave normal angle to the magnetic field is guided to the ground, then a ray injected at the same location with $-\theta_0$ WNA must also be ducted to the ground. In a duct with a smooth cross section, if rays injected with $\pm\theta_0$ WNA at the equator reach the ground, then rays with wavenormal angle θ satisfying the condition $-\theta_0 \leq \theta \leq +\theta_0$ will also reach the ground. The least restrictive condition for interhemispherical propagation is found by letting $\theta_0 \rightarrow 0$. That is, equatorial rays injected with 0° WNA at some point in the duct must reach the ground for interhemispheric propagation to be possible. A large part of this study is determining if such rays exist for a duct of specified size and enhancement.

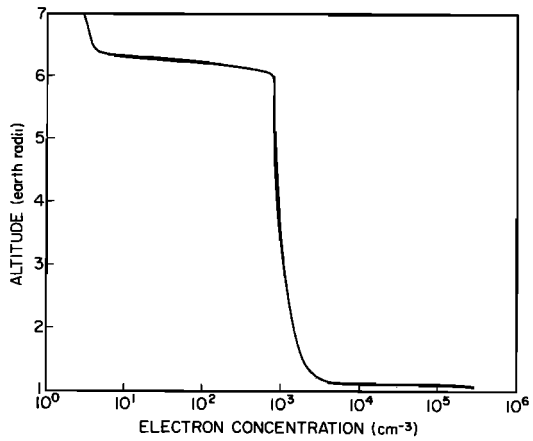

Fig. 2. Background plasma profile used for raytracing.

All of the ducts considered are centered on the $L = 4$ shell and are symmetric about the equator. Their enhancements range from 5% to 30%. The ducts are Gaussian-shaped with cross-L widths (i.e., standard deviations) σ_d ranging from 0.01 to 0.08 R_e at the equator. The duct endpoints extend down to 100-km altitude. The ducts are superimposed on a background plasma concentration in diffusive equilibrium with a plasmapause at 6 R_e, as shown in Figure 2. This plasma distribution represents a quiettime limit to the distributions derived from whistler measurements by *Park et al.* [1978].

Examples of the calculated ray paths are shown in Figure 2. Each frame includes a plot of the dipole magnetic field used to simulate the earth's field. The $L = 2$, 3, 4, and 5 field lines are outlined by heavy dashes.

The guiding of rays in a duct varies with initial wave normal angle and injection height. Wavenormals are indicated in the diagrams by short lines attached to the ray trajectories. Each frame of Figure 3 contains nine rays injected at one location at the equator with wave normal angles ranging from −20 to +20 degrees to the magnetic field. The raytracing is terminated when the ray is considered to be no longer trapped in a duct.

The ray is considered to be no longer guided by the duct if one of two conditions is satisfied. The first condition is that the ray be outside $2\sigma_d$ of the center of the duct. At this point the duct gradients are no longer sufficient to affect the ray trajectory. The second condition is that the magnitude of the ray WNA (with respect to the magnetic field) be greater than 45°. Even if the ray is inside the duct, if the magnitude of the WNA is greater than 45° the modest duct gradients used in this study cannot trap the wave. The definition of 'detrapping' is not critical because once the ray is no longer guided by the duct its distance from the center of the duct and its WNA rapidly increase.

Waves injected with the correct WNA angle at the optimum location are ducted to low altitudes (Figure 3*b*). Waves injected below (Figure 3*a*) or above (Figure 3*c*) the optimum location are only guided part way before they exit the duct. Thus the altitude where a ray leaves the duct as a function of the wave injection height and wavenormal angle is a measure of the VLF wave guiding properties of the duct.

Contour plots of this altitude as a function of the initial injection height and wavenormal angle are quantitative displays of the wave-trapping characteristics of the duct. The contour map for the propagation illustrated in Figure 3 is given in Figure 4. The initial wave normal angles are measured clockwise from the magnetic field direction. The initial wave injection height is the geocentric distance to the equatorial injection point in earth radii. The geocentric distance where the ray leaves the duct is also measured in earth radii.

The innermost contour in Figure 4 represents rays which are trapped to 1.25 R_e. Rays with equatorial injection heights and wave normal angles inside the shaded area of the central contour have a high probability of being received at the earth's surface. The actual penetration of the lower ionosphere by these rays depends on the duct endpoint heights and on irregularities in the ionosphere. Rays with initial conditions outside the 1.25 R_e contour leave the duct at too high an altitude for ground reception. Thus the wave-trapping contour plots provide a pictorial representation of the equator-to-ground transmission properties of a duct. The shape of this tranmission

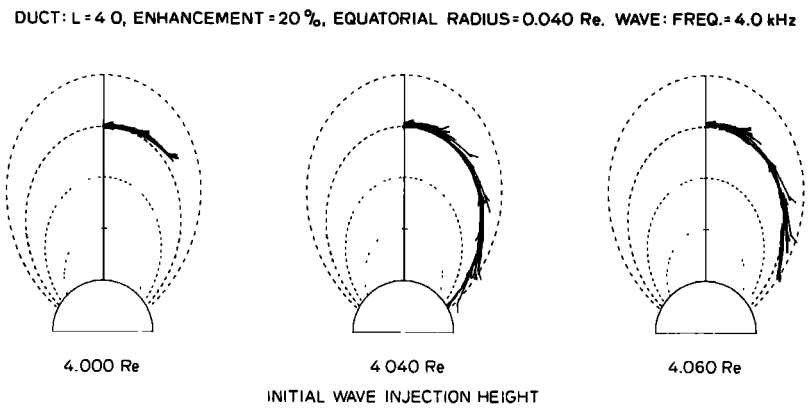

Fig. 3. Trajectories of equatorially injected rays. The altitude where they leave the $L = 4$ duct is a function of their initial position and wave normal angle.

characteristic depends on both the wave frequency and the physical shape of the duct.

As discussed previously, a necessary condition for interhemispheric propagation is that equatorially injected rays are guided to the earth's surface for an initial wavenormal angel of zero degrees. The shaded region of the wave-trapping contour map must contain the zero wave normal axis to allow interhemispheric propagation. This is the case in Figure 3 for wave injection between 4.02 and 4.04 R_e.

The wave-trapping contours change markedly as the wave frequency is increased above one-half of the equatorial gyrofrequency. In the raytracing examples for $L = 4$, the equatorial gyrofrequency is 13.76 kHz. The wave-trapping contours are illustrated in Figure 5 for a 20% enhancement duct with an equatorial width (σ_d) of 0.02 R_e. Propagation at 1, 4, 6, and 7.5 kHz is illustrated. The area inside the central contour decreases as the wave frequency approaches $f_{Heq}/2$ (6.88 kHz). Above this frequency the large shaded regions disappear, being repalced by small shaded patches where rays may be guided from the equator to the ground. One of these patches is located at an injection height of 4.01 R_e and a wave normal angle of $-5°$ for propagation at 7.5 kHz (Figure 5). Since the small shaded contour does not intersect the 0° wave normal angle line, this duct does not allow interhemispheric propagation for frequencies above $f_{Heq}/2$. Like this one, most ducts have a cutoff of $\Lambda = 0.5$.

By adjusting the size parameters of the duct, it is possible to relocate the shaded patches of 0° wave normal angle. If, for example, the duct enhancement factor is increased to 30% and the duct width (σ_d) is increased to 0.04 R_e, interhemispheric propagation is possible up to 7.5 kHz. A 7.5 kHz ray injected with zero wave normal angle at 4.02 R_e at the equator can be ducted to the earth's surface (Figure 6). Thus any interhemispheric propagation in this duct must involve rays which cross the equator at 4.02 R_e. The upper cutoff for this particular duct is 7.7 kHz ($\Lambda = 0.56$). Figure 7 illustrates another case of interhemispheric propagation. A 5% enhancement duct with an equatorial width (σ_d) of 0.01 R_e can guide VLF signals with frequencies above $0.6f_{Heq}$. At 8 kHz these signals cross the equator at 4.01 R_e with zero wave normal angle. In both cases, the ray path stays within one σ of the duct center.

Based on a study of these and similar contour maps, some conclusions are drawn about VLF propagation. The upper cutoff frequency of a whistler is usually $0.5f_{Heq}$, independent of the duct size and shape. The upper cutoff of super whistlers is a function of the physical structure of the duct in which they propagate. In general, Gaussian-shaped ducts with the same ratio of enhancement factor to equatorial radius have the same upper cutoff frequency above the half-gyrofrequency. Slight changes in the structure of a duct can produce large changes in its ability to guide rays with frequencies greater than $0.5f_{Heq}$. The cross section of ducts may change if the ducts are convected to different L shells by electric fields. Consequently, convecting ducts can lose (or gain) the ability to propagate super whistlers.

Ducted rays with frequencies above $f_{Heq}/2$ cross the equator above the center of the duct. Their exact position as they cross the equator is a function of the cut size and shape, and is within σ_d of the duct center.

One other factor can contribute to an apparently high whistler cutoff frequency. This is the deviation of the earth's field from a dipole field. A study by *Seely* [1977] has shown that the use of the dipole model leads to errors of a few percent in estimation of equatorial gyrofrequency. This small error cannot be used to explain the super whistler, diplaying a cutoff Λ

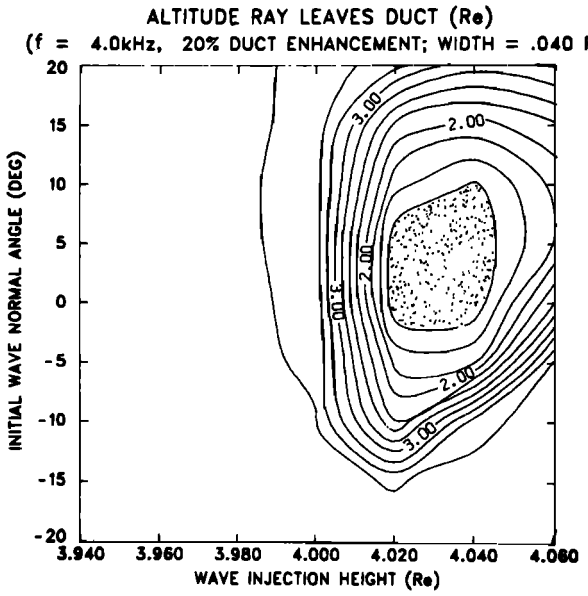

Fig. 4. Wave-trapping contour maps determined from the ray trajectories illustrated in Figure 2. Rays with initial conditions outside the shaded region are not ducted to the earth's surface. Contour lines indicate the geocentric distance where the ray is no longer trapped in a duct.

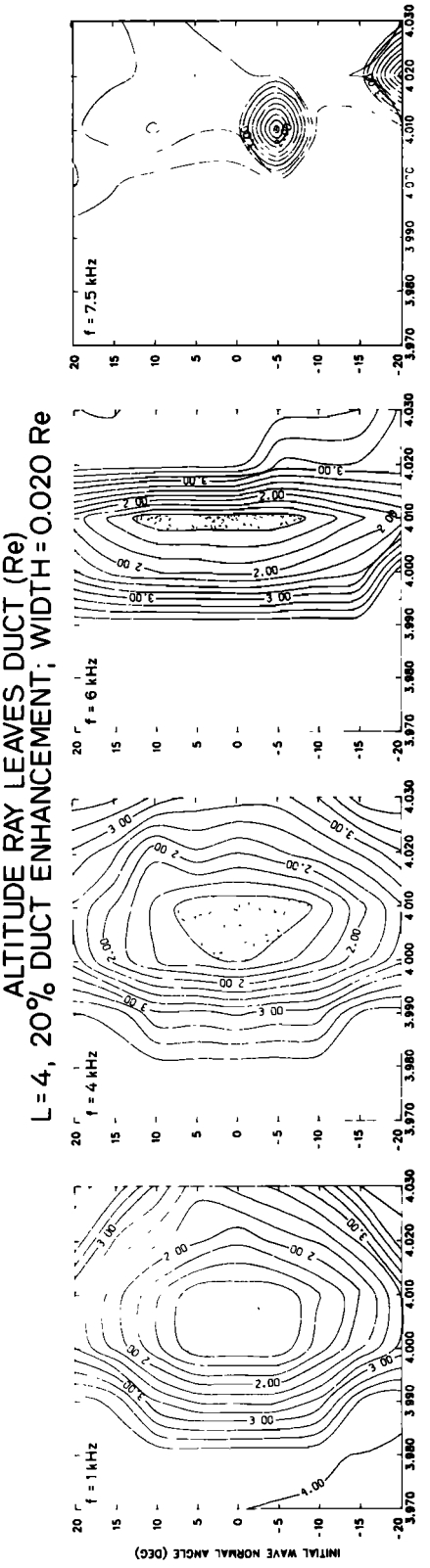

Fig. 5. Variation in wave-trapping contours as the frequency is changed. Above one-half the equatorial gyrofrequency (6.88 kHz), inter-hemispheric propagation is no longer possible.

greater than 0.6. Also, the super whistler has a noticeably higher cutoff than neighboring $\Lambda \cong 0.5$ whistlers. Consequently, the non-dipole nature of the geomagnetic field cannot account for the super whistler observations.

To summarize, there exists a family of ducts which allow interhemispheric propagation of VLF waves above one-half the equatorial gyrofrequency along the ducted propagation path. Future research should examine the relationship between the super whistler cutoff frequency and the physical structure of the super whistler duct.

3. Examples of Super Whistlers

Many examples of super whistlers can be found in the data taken inside the plasmapause at high geomagnetic latitudes. An early spectrogram of a super whistler recorded at Seattle on June 7, 1959, is illustrated in the textbook by *Helliwell* [1965, Figure 4–17]. The examples presented here have been carefully selected from recent measurements to present clear evidence of the super whistler phenomenon. All observed super whistlers occur among a spectrum of ordinary whistlers. Super whistlers are not triggered emissions because they are long-lived and repeatable.

Figure 8 illustrates a super whistler spectrogram taken at Siple on July 4, 1973. This extraordinary whistler was repeatedly seen between 1510 and 1525 UT. The spectrogram shows a number of whistlers propagating along neighboring ducts at differing L shells. All of the whistlers, except one, are cut off at the equatorial half-gyrofrequency along the path. The super whistler, however, extends to $\Lambda = 0.61$.

The next examples are taken from measurements made at Siple Station on June 28, 1975. Figure 9 illustrates a large number of whistlers from a single source, whose cutoffs all show $\Lambda \leq 0.5$, except for two. Super whistler B, with the low nose frequency, has $\Lambda = 0.61$ and was observed in the data for a period of 1 hour. The other super whistler (A) with $\Lambda = 0.64$ was observed from 2040 UT through 2330 UT.

One use of the super whistler is to 'tag' an individual propagation path among many. The super whistler can provide a clear, long-lasting measure of the changing magnetosphere. Another use of the super whistler is to provide information about the physical structure of the magnetosphere, as discussed in the next sections.

4. The Magnetospheric Shape Factor

As stated in the introduction, the nose whistler can be routinely analyzed to yield the path position (i.e., L shell) and equatorial plasma concentration of its propagation path. The extra information in the super whistler will be used to estimate the shape of the plasma distribution alon the propagation path near the equator. The plasma parameters are determined at the magnetic equator because this region has the largest influence on the whistler's dispersion (see appendix).

Most methods of whistler analysis assume that the whistler propagation path is confined to one field line at a fixed L shell. The actual path, however, is a twisting one such as shown in Figure 1. Fortunately, an increase in the average group velocity associated with the twisted path, to first order, compensates for the increased path length [*Smith,* 1960].

Consider the function $N(L, x)$, where L is the L shell parameter, $x = \sin \phi$ is the sine of the latitude, and N is the electron concentration at the location given by L and x. The function can be written as a Taylor series expansion about the equator ($x = 0$) at each L:

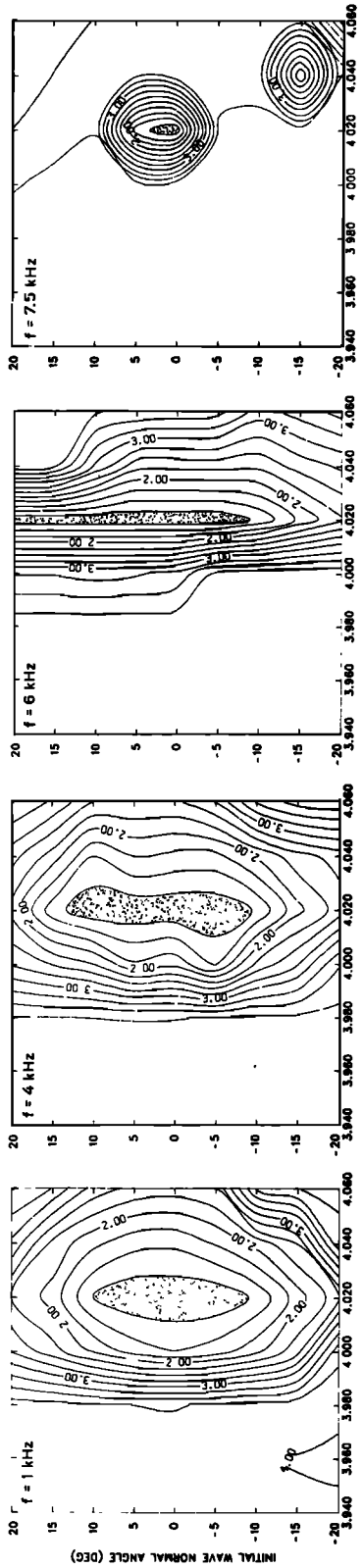

Fig. 6. Wave-trapping contours for a duct with a cutoff frequency of 717 kHz. Equatorial rays injected at 4.02 R_e with zero wave normal angle are guided below 1.25 R_e.

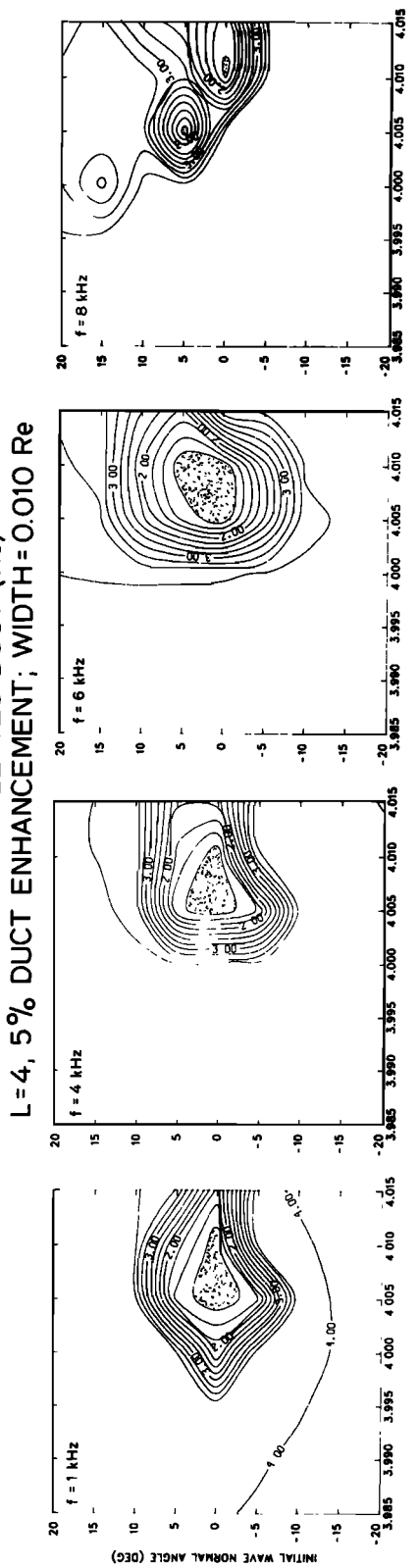

Fig. 7. Wave-trapping contours for a duct with a cutoff frequency greater than 8 kHz.

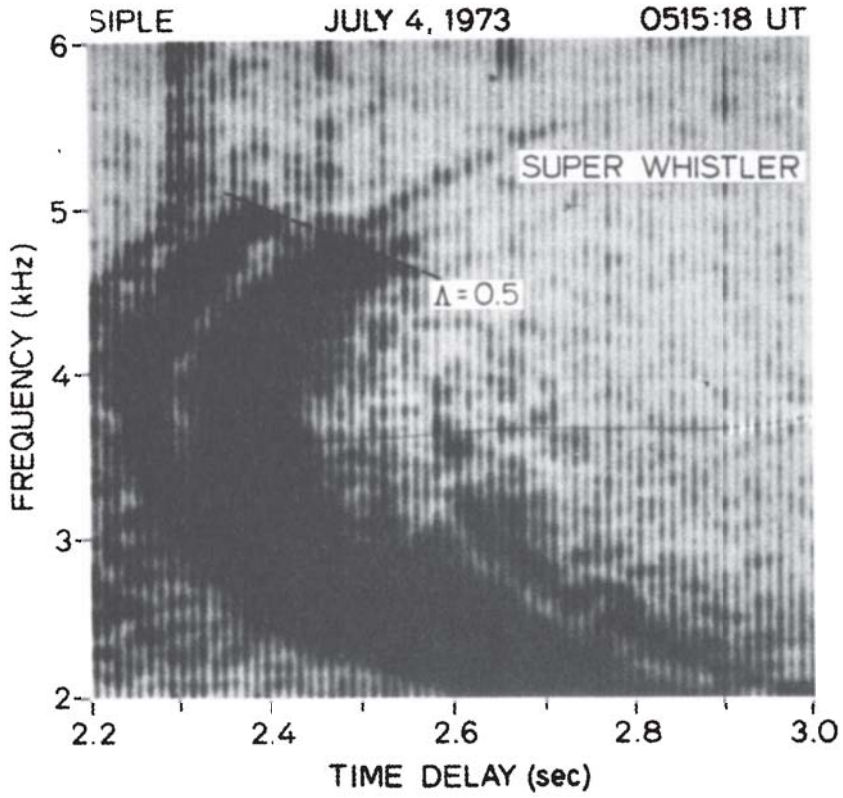

Fig. 8. Spectrogram showing a single super whistler.

$$N(L, x) = N(L, 0) + \frac{x^2}{2!}\frac{\partial^2 N}{\partial x^2}\bigg|_{x=0} + \frac{x^4}{4!}\frac{\partial^2 N}{\partial x^4}\bigg|_{x=0} + \cdots$$

The odd powers of x are dropped because the electron distribution is assumed to be symmetric about the equator. This equation suggests the following choice for the distribution shape factor

$$S = \frac{(\partial^2 N/\partial x^2)}{N}\bigg|_{x=0}$$

It is this parameter, S, which will be estimated from the super whistler measurements.

First, however, the physical interpretation of S is established. A theoretical model of the plasmasphere in an isothermal, diffusive equilibrium (DE) state has the form

$$N_{DE}(L, x) = N_{eq}\left\{\sum_i \xi_i \exp\left(-\frac{z}{H_i}\right) \cdot\left[\sum_i \xi_i \exp\left(-\frac{z_{eq}}{H_i}\right)\right]^{-1}\right\}^{1/2}$$

where N_{DE} is the electron concentration, geopotential height is

$$z = R_e L(1 - x_1^2)\left\{1 - \frac{(1 - x_1^2)}{1 - x^2} - \delta L^2(1 - x_1^2) \cdot[(1 - x^2)^2 - (1 - x_1^2)^2]\right\}$$

z_{eq} is z evaluated at $x = 0$; ξ_i is the fractional abundance of the ionic species with scale height $H_i = kT_i/m_i g$, with mass m_i and with temperature T; N_{eq} is the equatorial electron concentration, $x_1^2 = \sin\phi^2 = (1 - R_1/LR_e)$, ϕ_1, and R_1 are the geomagnetic latitude and geocentric radius, respectively, of the base of the DE model, g_1 is the gravitational acceleration at the point, $\delta = \Omega^2 R_e/2g_0$, Ω is the rotational speed of the earth, and g_0 is the gravitational acceleration at the earth's surface. The geopotential height z accounts for altitude variations in gravitational force and centrifugal forces due to corotation of the plasma with the earth [*Angerami and Thomas*, 1964]. The free parameters affecting the shape of the diffusive equilibrium plasma distribution are the temperature T and composition ξ_i as well as N_{eq} and L.

The normalized second derivative is evaluated to give the diffusive equilibrium shape parameter. The calculation is outlined as follows:

$$\frac{\partial^2 N_{DE}}{\partial x^2} = \frac{\partial^2 N_{DE}}{\partial z^2}\left(\frac{\partial z}{\partial x}\right)^2 + \frac{\partial N_{DE}}{\partial z}\frac{\partial^2 z}{\partial x^2}$$

$$\frac{\partial^2 N_{DE}}{\partial x^2}\bigg|_{x=0} = \frac{\partial N_{DE}}{\partial z}\bigg|_{x=0}\frac{\partial^2 z}{\partial x^2}\bigg|_{x=0}$$

since

$$\frac{\partial z}{\partial x}\bigg|_{x=0} = 0$$

$$\frac{\partial N_{DE}}{\partial z} = \frac{N_{eq}}{2}\left[\sum_i \frac{-\xi_i}{H_i}\exp\left(\frac{-z}{H_i}\right)\right] \cdot\left[\sum_i \xi_i \exp\left(\frac{-z}{H_i}\right)\sum_i \xi_i \exp\left(\frac{-z_{eq}}{H_i}\right)\right]^{-1/2}$$

$$\frac{\partial^2 z}{\partial x^2}\bigg|_{x=0} = R_e L(1 - x_1^2)^2[6\delta L^3 - 2]$$

Evaluation at $x = 0$ where $z = z_{eq}$ and substituting $1 - x_1^2 = R_1/R_e L$ yields

$$S_{DE} = \frac{\partial^2 N_{DE}}{\partial x^2}\bigg|_{x=0}\Big/ N_{eq} = \sum_i \frac{\xi_i}{H_i}\exp\left[-\frac{z_{eq}}{H_i}\right] \cdot\left\{\sum_i \xi_i \exp\left[-\frac{z_{eq}}{H_i}\right]\right\}^{-1}\frac{R_1^2}{R_0 L}[1 - 3\delta L^3]$$

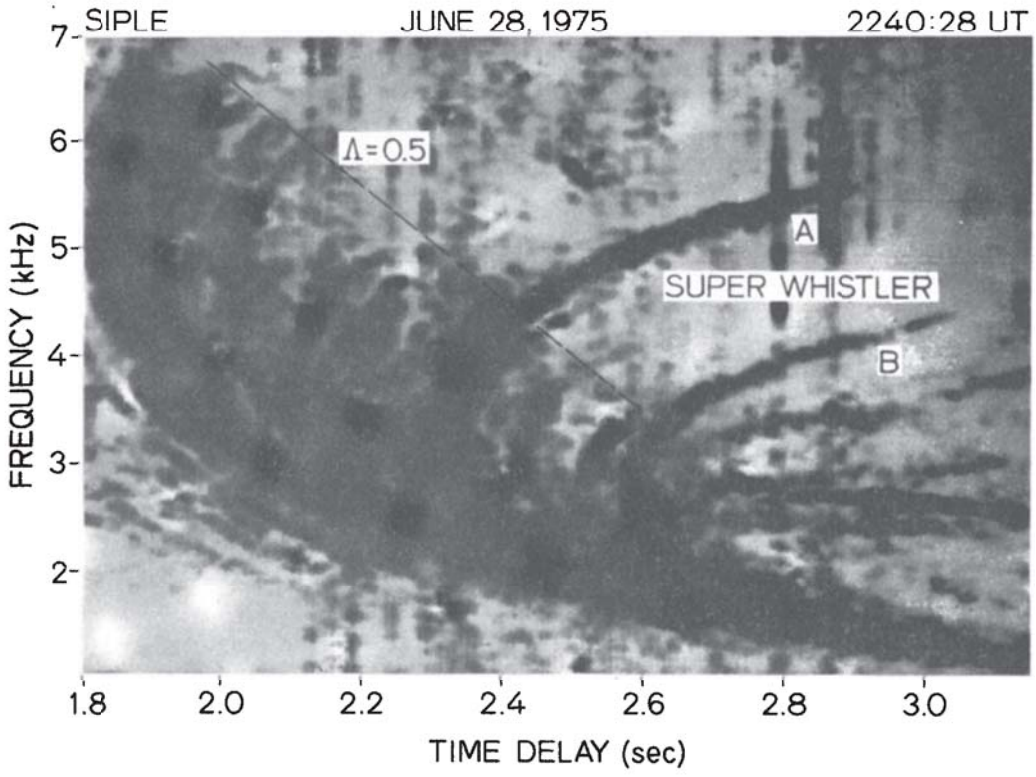

Fig. 9. Two super whistlers present among a spectrum of conventional whistlers.

For the case of one ionic species, H^+, this equation becomes

$$S_{DE} = \frac{R_1^2}{R_0 L}\left[\frac{1 - 3\delta L^3}{H}\right]$$

The shape parameter for the diffusive equilibrium model is a function of the L shell and the plasma temperature.

An alternative model of the plasma is the collisionless (CL) one given by *Angerami* [1966]:

$$N_{CL}(L, x) = N_{eq}\left\{\left[\exp\left(\frac{-z}{2H}\right) - \left(1 - \frac{B}{B_1}\right)^{1/2}\exp\left(\frac{-z}{2H(1 - B/B_1)}\right)\right] \cdot \left[\exp\left(\frac{-z_{eq}}{2H}\right) - \left(1 - \frac{B_{eq}}{B_1}\right)^{1/2}\exp\left(\frac{-z_{eq}}{2H(1 - B_{eq}/B_1)}\right)\right]^{-1}\right\}$$

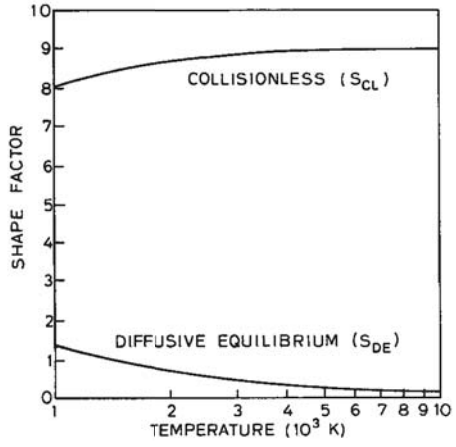

Fig. 10. Variation in the collisionless and diffusive-equilibrium shape factors with temperature. In all cases S_{CL} is much greater than S_{DE}.

where only one ionic species (H^+) is considered, z and H are the same as in the DE model, and B is the magnetic field strength given by

$$B = B_0(R_e/R)^3(3x^2 + 1)^{1/2}$$

B_0, B_1, and B_{eq} are the magnetic field strengths at the earth's surface, at the base of the collisionless model and at the equator, respectively. This model assumes that the collisionless plasma is being fed from a Maxwellian plasma with temperature T at geocentric radius R_1. Near the equator, $B \ll B_1$, and the CL model can be approximated by

$$N_{CL} \cong N_{eq}\exp\left[\frac{-(z - z_{eq})}{2H}\right]\frac{B}{B_{eq}}\frac{(H + z)}{(H + z_{eq})}$$

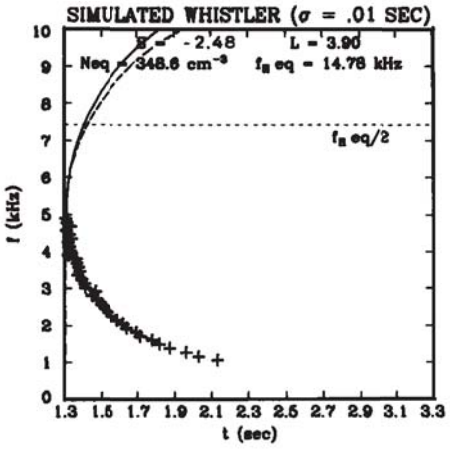

Fig. 11. Reconstructed whistler (solid curve) based on calculated samples with additive Gaussian noise. The dashed line is the actual whistler derived from the DE model with $L = 4$, $N_{eq} = 200$ cm^{-3}, and $S = 1.70$.

TABLE 1. Uncertainties in Plasma Parameters Derived From Simulated Whistlers With Additive Gaussian (σ = 0.01 s) Noise

	Diffusive Equilibrium Model			Collisionless Model		
	L	N_{eq}, cm^{-3}	S	L	N_{eq}, cm^{-3}	S
Actual parameters	4	200	1.70	4	200	8.55
Whistler cutoff						
$\Lambda = 0.35$	3.96 ± 0.06	267 ± 82	-0.32 ± 2.15	3.95 ± 0.07	250 ± 83	7.3 ± 1.32
$\Lambda = 0.5$	3.98 ± 0.04	227 ± 42	0.81 ± 1.04	3.98 ± 0.04	192 ± 25	8.55 ± 0.43
$\Lambda = 0.6$	4.00 ± 0.02	200 ± 15	1.37 ± 0.47	4.00 ± 0.02	186 ± 15	8.37 ± 0.23

Proceeding as with the *DE* model, the shape factor for the *CL* model is found to be

$$S_{CL} = \frac{\partial^2 N_{CL}}{\partial x^2}\bigg|_{x=0} \Big/ N_{eq} = 9 + \frac{(z_{eq} - H)}{H(H + z_{eq})} \frac{R_1^2}{R_0 L} [3\delta L^3 - 1]$$

A comparison of this expression with the one for the diffusive equilibrium shape factor yields the relationship

$$S_{CL} = 9 - \left[\frac{(z_{eq} - H)}{(z_{eq} + H)}\right] S_{DE}$$

The shape factor is a measure of the increase in the plasma concentration moving away from the equator down a field line. The collisionless model has a much more rapid increase in the plasma density off the equator than does the diffusive equilibrium model. Consequently, S_{CL} is considerably larger than S_{DE}. Figure 10 illustrates a typical variation in the *DE* and *CL* shape factors with temperatures ranging between 1000 and 10,000 K for the $L = 4$ models with the base of the plasma at $R_1 = 7370$ km.

The shape factor can take on values ranging from 0 to 9. A shape factor of zero represents a uniform distribution of plasma along a field line. This distribution occurs for the *DE* model if the temperature goes to infinity.

The shape factor of 9 is the limiting case for a collisionless model with an infinite source temperature. In this limit the plasma distribution takes a simple form

$$\lim_{T \to \infty} N_{CL} = N_{eq} \frac{B}{B_{eq}}$$

which is the gyrofrequency model [*Smith*, 1960].

The shape factor of the field-aligned plasma distribution may be estimated from super whistler measurements. The procedure, discussed in detail in the appendix, is outlined as follows. Assuming that the propagation is along a dipole field line L, the time versus frequency measurements are numerically fitted to the whistler group delay function. This function is an integral of the inverse of the whistler group velocity along the propagation path. The electron concentration along this path is expressed as an exponential power series in x:

$$N = \exp [2(p_1 + p_2 x^2 + p_3 x^4 + \cdots]$$

where $x = \sin \phi$, and $p_n (n = 1, 2, 3, \cdots, N)$ are parameters to be determined. The p_n and L parameters are adjusted to minimize the least-squares difference between the whistler measurements and the group delay function. The exponential power series was chosen as a model of the electron concentration because it has an exponential form similar to both the *DE* and *CL* models. It is also convenient for mathematical manipulations. The equatorial concentration and shape factor is found from the power series parameters:

$$N_{eq} = \exp (2p_1)$$

$$S = 4p_2$$

In practice, only the two parameters, p_1 and p_2, are determined using the least-squares procedure.

5. TESTING THE METHOD

Before applying the analysis to super whistler measurements, the procedure is tested on simulated whistlers. A model of the plasmasphere is used to generate the whistler time versus frequency samples. Zero-mean Gaussian noise is added to the samples yielding a set of test data. The L shell, equatorial concentration and shape factor is then estimated from the test data. The errors in these estimates are shown to decrease as the cutoff frequencies of the whistlers are increased.

In the tests, whistlers are simulated for propagation on the $L = 4$ field line in a diffusive equilibrium (*DE*) plasma or in a collisionless (*CL*) plasma with an equatorial concentration of 200 electroms/cm^3, and a temperature of 1600°K. The *DE* model has relative H^+, He^+, and O^+ concentrations of 0.5, 0.1, and 0.4, respectively, at 1000 km altitude. The *DE* distribution and the *CL* distribution have shape factors of $S = 1.70$ and $S = 8.55$, respectively. Gaussian noise with a standard deviation (σ) of 0.01 s is added to all calculated whistlers. Different samples of additive noise lead to different values of parameters being derived from the whistlers.

Figure 11 illustrates the results for analysis of a *DE*-model whistler with a cutoff of $\Lambda = 0.35$. This nose whistler yields parameter estimates of $L = 3.9$, $N_{eq} = 349$, and $S = -2.40$, corresponding to the solid curve in the figure. The dashed curve is calculated using the actual model parameters ($L = 4$, $N_{eq} = 200$, and $S = 1.70$).

The $\Lambda = 0.35$ whistler does not provide enough information to allow accurate determination of the plasma shape factors. Also, the example shows greater deviation of the estimated whistler curve from the actual whistler curve as the wave frequency is increased.

The results of similar tests are given in Table 1. The estimated parameters and their uncertainties are tested for whistler cutoffs of $\Lambda = 0.35$, 0.5, and 0.6. The error in the estimates decreases as the cutoff frequency is increased. The analysis of the simulated super whistler ($\Lambda = 0.6$) provides an accurate retrieval of the plasma concentration parameters. In general, whistlers with $\Lambda = 0.35$ or greater contain sufficient information for reliable estimations of L and N_{eq}. The shape factor, however, can only be reliably determined from whistlers with $\Lambda > 0.5$.

Errors in estimation of the plasma parameters are also introduced by inaccuracies in the location of the causative spheric. Figure 12 illustrates the magnitude of these errors. A simulated whistler ($\Lambda = 0.6$) is calculated using the *DE* model

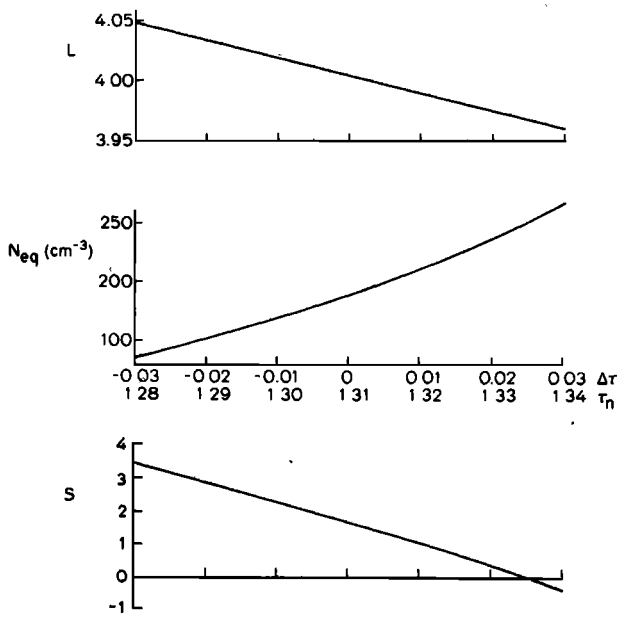

Fig. 12. Effect of spheric location error ($\Delta\tau$) on parameters estimated from a super whistler.

(L = 4, N_{eq} = 200, S = 1.70). This whistler has a nose delay time of 1.31 s. A spheric location error of $\Delta\tau$ s will produce an apparent nose time of 1.31 + $\Delta\tau$ s. The effect of delaying all of the whistler frequency components by $\Delta\tau$ is shown in the figure. A spheric error of 0.01 s produces an absolute error of 0.02 in L, of 22 cm^{-3} in N_{eq}, and of 0.61 in S.

Consequently, a fundamental limitation to the super whistler analysis is the error in spheric location. One method of decreasing this error is by superimposing and analyzing a number of super whistlers which have all propagated on the same duct. Also, two-hop super whistlers measured at conjugate stations would be ideal for this analysis.

6. Experimental Results

Using the tools developed in the previous sections, experimental measurements of super whistlers are analyzed to provide estimates of path position, equatorial concentration and shape factor. These parameters will be discussed in terms of the physical processes in the plasmasphere. A comparison is made between the estimates provided by analysis of conventional whistlers and those determined from super whistler analysis.

The first example is taken from whistler recordings made at Siple on July 4, 1973. Whistler measurements made on this day have been previously examined in detail by *Carpenter* [1978]. This was the first geomagnetically quiet day (Σkp = 9) following a 6-day period of disturbance. Consequently, the plasma on this day is expected to be in a non-diffusive equilibrium state due to its recovery after a substorm.

Eighty-five samples of four super whistlers near 0515 UT are superimposed and analyzed, giving the results displayed in Figure 13*a*. The least-squares fit produced the solid curve. The standard deviation of the measured points from this curve is .0088 s. A shape factor of 3.71 was extracted from measurements, indicating that the plasma is between a *CL* and a *DE* state. Analysis of super whistlers taken 10 min later (Figure 13*b*) shows an outward convection of the plasma duct and in increase in the shape factor (S = 4.79).

The second example is taken from super whistler measurements made on June 28, 1975. This was the last day of a geomagnetic quiet period (Σkp < 11) which lasted for 11 days. At this time the plasma should have reached a diffusive equilibrium state.

Two super whistlers, on two different paths, were simultaneously present in the measurements taken at 2240:28 UT on June 28, 1975. The lower-latitude super whistler (A in Figure 9) yields a shape factor S = 2.27 (see Figure 14*a*). This low value indicates that the plasma distribution is near diffusive equilibrium. The higher-latitude super whistler (B in Figure 9) yields a shape factor of 2.92 (Figure 14*b*) indicating a plasma distribution between a *DE* and a *CL* state. Thus the outer layer of plasma may not have yet relaxed to a diffusive equilibrium state.

The state of the plasmasphere will affect the estimates of equatorial plasma concentration based on whistler measurements. The conventional analysis technique [*Park*, 1972] has been applied to the June 28, 1978, whistlers. The results of this analysis are plotted in Figure 15. Also plotted are two estimates of N_{eq} based on super whistler analysis. The results derived from the low-latitude super whistler (A) are in good agreement with the conventional analysis (A'). The *DE* shape factor for super whistler (A) is consistent with the conventional analysis. Since super whistler (B) is not produced by propagation in a *DE* plasma, the equatorial concentration of its path is overestimated by the conventional analysis (B').

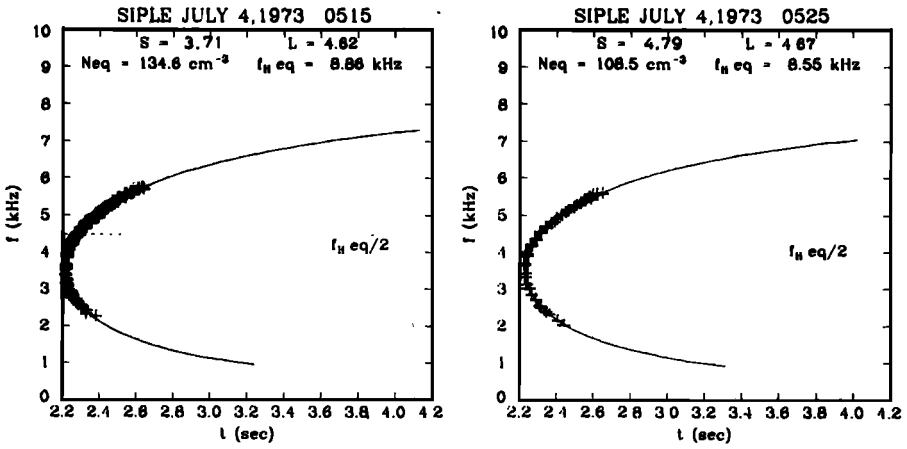

Fig. 13. Analysis of July 4, 1973, super whistlers. One sample of these data is illustrated in Figure 7.

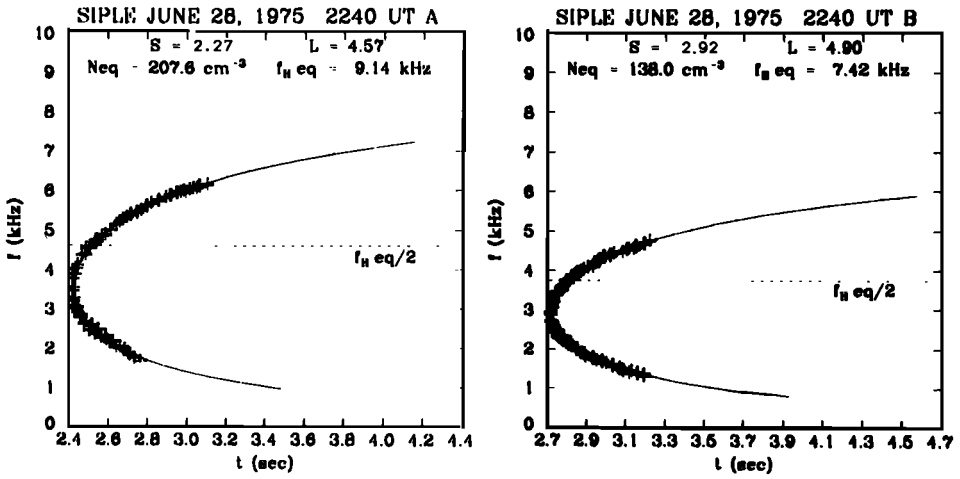

Fig. 14. Analysis of the June 28, 1975, super whistlers illustrated in Figure 8.

7. Concluding Remarks

Calculations of ray trajectories in Gaussian-shaped ducts provide one explanation for whistlers which have cutoff frequencies significantly greater than one-half the equatorial electron gyrofrequency. A ducted ray propagates upward until it reaches a point where the wave frequency equals 0.5 the local electron gyrofrequency. It then propagates in an unducted mode. If the ray crosses the equator with zero wave normal angle with respect to the magnetic field, it will then propagate on a reciprocal path in the conjugate hemisphere to be ducted at low latitudes.

This type of ducting occurs only for ducts of specific sizes and enhancements. The relationship between the super whistler cutoff frequency and the physical properties of the whistler duct should be examined in greater detail. If this relationship is firmly established, the super whistler could provide knowledge about the distribution irregularities in the magnetosphere.

Analysis of super whistlers can extend our knowledge of the plasmasphere by providing more information than does analysis of conventional whistlers. Specifically, super whistler analysis provides information on the distribution of the plasma along the magnetic field near the equator. Such information may be used to validate theoretical models of the plasmasphere. Most quantitative studies of plasma flow in the magnetosphere [e.g., *Murphy et al.*, 1976] assume near-equilibrium conditions. Consequently, the diffusion equation is used in these solutions. The plasma distributions obtained from super whistlers suggest that the state of the plasma may be far from equilibrium during disturbed times. In this case, higher-order transport equations are required to describe the plasma [e.g., *Schunk*, 1977].

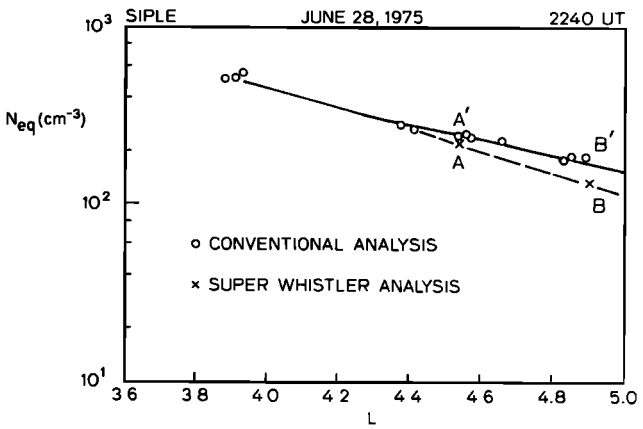

Fig. 15. Equatorial plasma profiles estimated by conventional and super whistler techniques. Deviation from diffusive equilibrium for L greater than 4.6 accounts for the difference between the two methods.

The plasma distribution affects the generation of VLF emissions produced by wave-particle interactions in the magnetosphere. *Helliwell* [1970] discusses the relationship between a plasma index N and the length of the interaction region near the equator. Helliwell's plasma index is the shape factor S (defined in section 4) divided by 18. Plasma gradients are also important in the theory of triggered VLF emissions by *Nunn* [1974]. Thus super whistler measurements yield information that is useful in calculating the resonant interaction of VLF waves with high-energy radiation belt electrons.

Several areas of future research are suggested. The super whistler data base should be extended. The conclusions made here, based on only four examples, should be checked. Simplification of the super whistler analysis should be attempted.

Appendix

Approximation of a Nonlinear Function by the Method of Least-Squares

A procedure for fitting a nonlinear function to a set of paired data is outlined. Consider a function with independent variable f and $N + 1$ parameters $(p_0, p_1, \cdots, p_N)$

$$t(f; p_0, p_1, \cdots, p_N) = t(f; \bar{p}) \tag{A1}$$

where the matrix notation, $\bar{p} = (p_0, p_1, \cdots, p_N)^T$, has been introduced. The problem is to determine the parameters, $\bar{p}$, so that (A1) approximates a set of data pairs

$$(t_1, f_1), (t_2, f_2), \cdots, (t_M, f_M)$$

The least-squares solution to this problem is minimization of the norm

$$L_2(\bar{p}) \equiv \sum_{m=1}^{M} [t_m - t(f_m; \bar{p})]^2 \tag{A2}$$

$L_2(\bar{p})$ becomes as small as possible for the condition

$$\frac{\partial L_2(\bar{p})}{\partial p_n} = 0$$

or

$$\sum_{m=1}^{M} [t_m - t(f_m; \bar{p})] \frac{\partial t(f_m; \bar{p})}{\partial p_n} \equiv G_n(\bar{p}) = 0 \qquad (A3)$$

$$n = 0, 1, \cdots, N$$

This nonlinear system of $N + 1$ equations with $N + 1$ unknowns is compactly written in vector notation: $\bar{G}(\bar{p}) = 0$, where $\bar{G}(\bar{p}) = [G_0(\bar{p}), G_1(\bar{p}), \cdots, G_N(\bar{p})]^T$. Newton-Raphson's method (generalized to $N + 1$ dimensions) is used for solving (A3) [*Dahlquist et al.*, 1974]. The solution vector $\bar{p}$ is found by iteration

$$\bar{G}'(\bar{p}^{(k)})(\bar{p}^{(k+1)} - \bar{p}^{(k)}) + \bar{G}(\bar{p}^{(k)}) = 0 \qquad (A4)$$

where $\bar{p}^{(k)}$ is the estimate of $\bar{p}$ at iteration k and $\bar{G}'(\bar{p}^{(k)})$ is a $(N + 1) \times (N + 1)$ square matrix with elements $\bar{G}_{nl}'(\bar{p}^{(k)}) = \partial G_n(\bar{p}^{(k)})/\partial p_l$. Explicitly,

$$G_{nl}'(\bar{p}^{(k)}) = \sum_{m=1}^{M} \left[[t_m - t(f_m; \bar{p}^{(k)})] \frac{\partial^2 t(f_m; \bar{p}^{(k)})}{\partial p_n \partial p_l} - \frac{\partial t(f_m; \bar{p}^{(k)})}{\partial p_n} \frac{\partial t(t_m; \bar{p}^{(k)})}{\partial p_l} \right] \qquad (A5)$$

The linear system of equations by (A4) may be solved for $p^{(k+1)}$ by using the standard methods of linear algebra if the Jacobian matrix, $\bar{G}'(\bar{p}^{(k)})$, is nonsingular. The iteration processes will converge to the correct solution provided that the initial trial solution $\bar{p}^{(0)}$ lies sufficiently close to $\bar{p}$.

Application to the Whistler
Time Delay Function

The procedure outlined in the previous section is applied to the analysis of whistlers. The group delay for a whistler wave propagating along a geomagnetic field line is

$$t(f) = \frac{1}{2c} \int_{\text{path}} \frac{f_p f_H \, ds}{f^{1/2}(f_H - f)^{3/2}} \qquad (A6)$$

where f is the wave frequency, f_p the plasma frequency, f_H the gyrofrequency, c the speed of light, and ds an element of path length along the field line. The assumptions used in deriving (A6) are given by *Smith* [1960] and *Park* [1972]. The method described here may be applied to more accurate representations of $t(f)$ but (A6) is sufficient for analysis of whistlers under normal conditions in the magnetosphere.

A centered dipole is assumed for the geomagnetic field. With this approximation, the gyrofrequency is given by

$$f_H = f_{HOEQ} \frac{(1 + 3 \sin^2 \phi)^{1/2}}{L^3 \cos^6 \phi} \qquad (A7)$$

where f_{HOEQ} is the gyrofrequency at the earth's equator on the surface, L is the distance to the equatorial point on the field line divided by the earth's radius (R_e), and ϕ is the magnetic latitude. This variation in the gyrofrequency causes the largest contribution to the whistler's propagation time to be from the plasma at or near the magnetic equator. The plasma frequency is

$$f_p = \frac{e}{2\pi(\epsilon_0 m)^{1/2}} N_e^{1/2} \qquad (A8)$$

where e is the elementary charge, $\pi = 3.1415926$, ϵ_0 the permittivity constant, m the electron rest mass, and N_e the electron density in m^{-3}. A power series model is used for variation of electron concentration with latitude

$$N_e = \exp\left[2 \sum_{n=1}^{N} p_n x^{2(n-1)}\right] \qquad (A9)$$

where $x = \sin \phi$. Only even powers of x are included in the power series because the densities are assumed to be symmetric about the equator.

The path is confined to a field line (with parameter L) extending from one hemisphere to the conjugate hemisphere. The latitude at the endpoints of the path is given by

$$\cos^2 \phi_1 = \frac{R_1}{R_e L} \qquad (A10)$$

where R_1 is the geocentric distance to the endpoints.

Using (A7)–(A10), (A6) is transformed to the form

$$t(f) = t(f; \bar{p}) = \int_0^{x_1} \mathcal{J}(\bar{p}, x) dx \qquad (A11)$$

where

$$\mathcal{J}(\bar{p}, x) = \beta \frac{p_0^{5/2}}{f^{1/2}} \exp\left[\sum_{n=1}^{N} p_n x^{2n}\right] A2\left(\frac{A_1}{B_2 - B_1}\right) \qquad (A12)$$

$A_1 = 1 - x^2$, $A_2 = 1 + 3x^2$, $B_1 = f p_0^3 A_0^3$, $B_2 = f_{HOEQ} A_2^{1/2}$, $x_1 = \sin \phi_1$, $p_0 = L$, and $\beta = eR_e f_{HOEQ}/2\pi(\epsilon_0 m)^{1/2} c = 1.665 \times 10^8$.

Given a whistler time delay measurement (t_m) for each frequency (f_m), (A11) can be used in conjunction with (A3), (A4), and (A5) to yield least-square estimates of p_0 (the L shell parameter) and $p_1, p_2, \cdots, p_N$ (the density model parameters). The derivatives of (A11) required for the analysis are given as follows:

$$\frac{\partial t(f; \bar{p})}{\partial p_0} = \mathcal{J}(\bar{p}, x_1) \frac{\partial x_1}{\partial p_0} + \int_0^{x_1} \mathcal{J}(\bar{p}, x) \mathcal{K}(p_0, x) dx \qquad (A13)$$

where

$$\frac{\partial x_1}{\partial p_0} = \frac{R_1}{2 x_1 R_e p_0^2}$$

and

$$\mathcal{K}(p_0, x) = \left[\frac{\partial \mathcal{J}(\bar{p}, x)/\partial p_0}{\mathcal{J}(\bar{p}, x)}\right] = \frac{5}{2p_0} + \frac{9}{2} \frac{B_1}{p_0(B_2 - B_1)} \frac{\partial t(f; \bar{p})}{\partial p_n}\bigg|_{n \neq 0} + \int_0^{x_1} \mathcal{J}(\bar{p}, x) x^{2(n-1)} dx \qquad (A14)$$

$$\frac{\partial^2 t(f; \bar{p})}{\partial p_0^2} = \mathcal{J}(\bar{p}, x_1)\left\{2\mathcal{K}(p_0, x_1) + \mathcal{L}(\bar{p}, x_1) \frac{\partial x_1}{\partial p_0} + \frac{\partial^2 x_1}{\partial p_0^2}\right\} + \int_0^{x_1} [\mathcal{K}^2(p_0, x) + \mathcal{M}(p_0, x)] \mathcal{J}(\bar{p}, x) dx \qquad (A15)$$

where

$$\mathcal{L}(\bar{p}, x_1) = \sum_{n=1}^{N} 2(n-1) p_n x_1^{2n-3} + \frac{6x_1}{A_2} + \frac{3}{2} \frac{x_1[B_2(-4 - A_2)/A_2 - 4B_1]}{(B_2 - B_1)A_1}$$

$$\mathcal{M}(p_0, x) = -\frac{5}{2p_0^2} + \frac{9}{2} \frac{B_1(2B_2 + B_1)}{p_0^2(B_2 - B_1)^2}$$

and

$$\frac{\partial^2 x_1}{\partial p_0^2} = \frac{-R_1}{x_1 R_e p_0^3}\left[1 + \frac{R_1}{4x_1^2 R_e p_0}\right]$$

$$\left.\frac{\partial^2 t(f;\bar{p})}{\partial p_0 \partial p_n}\right|_{n\neq 0} = \mathcal{J}(\bar{p}, x_1)\frac{\partial x_1}{\partial p_0}x^{2(n-1)} \cdot \int_0^{x_1}\mathcal{J}(\bar{p}, x)\mathcal{K}(p_0, x)x^{2(n-1)}dx \quad (A16)$$

$$\left.\frac{\partial^2 t(f;\bar{p})}{\partial p_n \partial p_l}\right|_{\substack{n\neq 0\\ l\neq 0}} = \int_0^{x_1}\mathcal{J}(\bar{p}, x)x^{2(n+l-2)}\,dx \quad (A17)$$

The initial trial solution, $\bar{p}^{(0)}$, is found as follows. Approximate values of L and N_{eq} (electron density at the equator) are determined from the whistler nose frequency and time delay [see *Park*, 1972]. The initial values for p_0 and p_1 are given by

$$p_0^{(0)} = L \qquad p_1^{(0)} = \tfrac{1}{2}\log_e(N_{eq}) \quad (A18)$$

The least-squares method will produce estimates of $\bar{p}$ by iteration with (A4). With $N = 1$,

$$\begin{bmatrix} G_{00}'(p_0^{(k)}, p_1^{(k)}) & G_{01}'(p_0^{(k)}, p_1^{(k)}) \\ G_{10}'(p_0^{(k)}, p_1^{(k)}) & G_{11}'(p^{(k)}, p^{(k)}) \end{bmatrix}\begin{bmatrix}\Delta p_0 \\ \Delta p_1\end{bmatrix} + \begin{bmatrix} G_0(p_0^{(k)}, p_1^{(k)}) \\ G_1(p_0^{(k)}, p_1^{(k)})\end{bmatrix}$$

where $\Delta p_n = p_n^{(k+1)} - p_n^{(k)}$. The iteration terminates when

$$\max\left[\frac{\Delta p_n}{p_n}, n = 0, 1, \cdots, N\right] < \epsilon \quad (A19)$$

where $\Delta p_n/p_n$ is the relative error and $\epsilon \ll 1$ is the acceptable error level.

After the iteration process converges to a set of parameters, N is incremented by one. The initial parameters for a new iteration are given by

$$p_n^{(0)} = p_n, n = 0, 1, \cdots, N-1$$

$$p_N^{(0)} = 0$$

The accuracy of the least-squares approximation with each new set of parameters is determined from (A2). Computation is halted when the addition of another parameter does not decrease the value of $L_2(\bar{p})$. The number of parameters obtained is a function of the accuracy and frequency range of the whistler time delay measurements.

Acknowledgments. The author thanks C. G. Park, D. L. Carpenter, and T. R. Miller for pointing out excellent examples of super whistlers in the data. The encouragement and advice from R. A. Helliwell and T. F. Bell, as well as the aforementioned personnel, is gratefully acknowledged. This research was supported in part by the Office of Naval Research under grant N00014-76-C-0689. Data acquisition in Antarctica has been supported by the National Science Foundation, Division of Polar Programs, under grant DPP76-82646. Some data analysis has been supported by the National Science Foundation, Atmospheric Sciences Section, under grant ATM75-07707.

The Editor thanks M. J. Rycroft and another referee for their assistance in evaluating this paper.

REFERENCES

Angerami, J. J., A whistler study of the distribution of thermal electrons in the magnetosphere, *SEL-66-017*, Radioscience Lab., Stanford Univ., Stanford, Calif., May 1966.

Angerami, J. J., and J. O. Thomas, Studies of planetary atmospheres, 1, The distribution of electrons and ions in the earth's exosphere, *J. Geophys. Res., 69*, 4537, 1964.

Bernard, L. C., A new nose extension method for whistler, *J. Atmos. Terr. Phys., 35*, 871, 1973.

Bernhardt, P. A., and C. G. Park, Protonospheric-ionospheric modeling of VLF ducts, *J. Geophys. Res., 82*, 5222, 1977.

Carpenter, D. L., Ducted whistler-mode propagation in the magnetosphere: A half-gyrofrequency upper intensity cutoff and some associated wave growth phenomena, *J. Geophys. Res., 73*, 2919, 1968.

Carpenter, D. L., New whistler evidence of a dynamo origin of electric fields in a quiettime plasmasphere, *J. Geophys. Res., 83*, 1588, 1978.

Corcuff, P., Méthodes d'analyse des sifflements électroniques, 1, Application à des sifflements théoriques, *Ann. Geophys., 33*, 443, 1977.

Corcuff, P., Y. Corcuff, and G. Tarcsai, Méthodes d'analyse des sifflements électronique, 2, Application à des sifflements observés au sol, *Ann. Geophys., 33*, 455, 1977.

Dahlquist, D., A. Björck, and N. Anderson, *Numerical Methods*, Prentice Hall, Englewood Cliffs, N. J., 1974.

Dowden, R. L., and G. M. Allcock, Determination of nose frequencies of non-nose whistlers, *J. Atmos. Terr. Phys., 33*, 1125, 1971.

Helliwell, R. A., *Whistlers and Related Ionospheric Phenomena*, Stanford University Press, Stanford, Calif., 1965.

Helliwell, R. A., Intensity of discrete VLF emissions, in *Particles and Fields in the Magnetosphere*, edited by B. M. McCormac, p. 292, D. Reidel, Dordrecht, Netherlands, 1970.

Ho, D., and L. C. Bernard, A fast method to determine the nose frequency and minimum group delay of a whistler when the causitive spheric is unknown, *J. Atmos. Terr. Phys., 35*, 881, 1973.

Murphy, J. A., G. J. Bailey, and R. J. Moffett, Calculated daily variations of O^+ and H^+ at mid-latitudes, 1, Protospheric replenishment and F-region behavior at sunspot minimum, *J. Atmos. Terr. Phys., 38*, 351, 1976.

Nunn, D., A self-consistent theory of triggered VLF emissions, *Planet. Space Sci., 22*, 349, 1974.

Park, C. G., Methods of determining electron concentrations in the magnetosphere from nose whistlers, *Tech. Rep. 3454-1*, Radioscience Lab., Stanford Univ., Stanford, Calif., 1972.

Park, C. G., D. L. Carpenter, and D. B. Wiggin, Electron density in the plasmasphere: Whistler data on solar cycle, annual, and diurnal variations, *J. Geophys. Res., 83*, 3137, 1978.

Schunk, R. W., Mathematical structure of transport equations for multispecies flows, *Rev. Geophys. Space Phys., 15*, 429, 1977.

Seely, N. T., Whistler propagation in a distorted quiet-time model magnetosphere, *Tech. Rep. 3472-1*, Radioscience Lab., Stanford Univ., Stanford, Calif., Aug. 1977.

Smith, A. D., I. D. Smith, and K. Bullough, Methods of determining nose-frequency and minimum group delay, *J. Atmos. Terr. Phys., 37*, 1179, 1975.

Smith, R. L., The use of whistlers in the study of the outer ionosphere, *Tech. Rep. 6*, Radioscience Lab., Stanford Univ., Stanford, Calif., July 1960.

Smith, R. L., R. A. Helliwell, and I. Yabroff, A theory of trapping of whistlers in field-aligned columns of enhanced ionization, *J. Geophys. Res., 65*, 815, 1960.

Strangeways, H. J., An investigation of the propagation of whistlers in magnetospheric ducts by means of ray-tracing, curve-fitting, and direction-finding techniques, Ph.D. thesis, Dep. of Phys., Univ. of Southampton, Southhampton, England, Nov. 1977.

Tarcsai, G., Routine whistler analysis by means of accurate curve fitting, *J. Atmos. Terr. Phys., 37*, 1447, 1975.

Walter, F., Non-ducted VLF propagation in the magnetosphere, *Tech. Rep. 3418-1*, Radioscience Lab., Stanford Univ., Stanford, Calif., Oct. 1969.

(Received October 19, 1978;
revised February 26, 1979;
accepted March 27, 1979.)